The Astrophysical Journal, 719:1859–1871, 2010 August 20 doi:10.1088/0004-637X/719/2/1859

DEBRIS DISKS OF MEMBERS OF THE BLANCO 1 OPEN CLUSTER*,†

John R. Stauffer[1], Luisa M. Rebull[2], David James[3], Alberto Noriega-Crespo[1], Steven Strom[4], Scott Wolk[5], John M. Carpenter[6], David Barrado y Navascues[7,8], Giusi Micela[9], Dana Backman[10], and P. A. Cargile[11]
[1] Spitzer Science Center, Caltech 314-6, Pasadena, CA 91125, USA
[2] Spitzer Science Center, Caltech 220-6, Pasadena, CA 91125, USA
[3] Physics and Astronomy Department, University of Hawaii at Hilo, Hilo, HI 96720, USA
[4] National Optical Astronomy Observatories, Tucson, AZ 85721, USA
[5] Harvard-Smithsonian Center for Astrophysics, 60 Garden St., Cambridge, MA 02138, USA
[6] Astronomy Department, Caltech, Pasadena, CA 91125, USA
[7] Calar Alto Observatory, Centro Astronómico Hispano Alemán, C/Jesús Durbán Remón, E-04004 Almería, Spain
[8] LAEX, Depto. Astrofísica, Centro de Astrobiología (INTA-CSIC) E-28691 Villanueva de la Cañada, Spain
[9] INAF-Osservatorio Astronomico di Palermo Giuseppe S. Vaiana, Piazza Parlamento 1, 90134 Palermo, Italy
[10] Stratospheric Observatory for Infrared Astronomy and SETI Institute, 515 North Whisman Road, Mountain View, CA 94043, USA
[11] Department of Physics and Astronomy, Vanderbilt University, Nashville, TN 37235, USA
Received 2009 July 8; accepted 2010 June 28; published 2010 August 4

ABSTRACT

We have used the *Spitzer Space Telescope* to obtain Multiband Imaging Photometer for *Spitzer* (MIPS) 24 μm photometry for 37 members of the ∼100 Myr old open cluster Blanco 1. For the brightest 25 of these stars (where we have 3σ uncertainties less than 15%), we find significant mid-IR excesses for eight stars, corresponding to a debris disk detection frequency of about 32%. The stars with excesses include two A stars, four F dwarfs, and two G dwarfs. The most significant linkage between 24 μm excess and any other stellar property for our Blanco 1 sample of stars is with binarity. Blanco 1 members that are photometric binaries show few or no detected 24 μm excesses whereas a quarter of the apparently single Blanco 1 members do have excesses. We have examined the MIPS data for two other clusters of similar age to Blanco 1—NGC 2547 and the Pleiades. The AFGK photometric binary star members of both of these clusters also show a much lower frequency of 24 μm excesses compared to stars that lie near the single-star main sequence. We provide a new determination of the relation between the $V - K_s$ color and $K_s - [24]$ color for main sequence photospheres based on Hyades members observed with MIPS. As a result of our analysis of the Hyades data, we identify three low mass Hyades members as candidates for having debris disks near the MIPS detection limit.

Key words: open clusters and associations: individual (Blanco 1) – stars: low-mass

Online-only material: color figure

1. INTRODUCTION

The past two decades have witnessed tremendous progress in understanding circumstellar disk formation and early evolution. With new results primarily from the *Spitzer Space Telescope* (Werner et al. 2004) and its Multiband Imaging Photometer for *Spitzer* (MIPS; Rieke et al. 2004) instrument, we are beginning to understand the diversity of old debris disk systems as a function of stellar mass (Rieke et al. 2005; Beichman et al. 2006; Bryden et al. 2006; Carpenter et al. 2009). But the transition between gas-rich primordial circumstellar accretion disks and mature planetary systems such as our own remains a mystery. What fraction of young solar mass stars have debris disks, and how does that fraction depend in detail on age? How do the properties of these disks depend on stellar metallicity or stellar mass? Does debris disk formation or evolution depend on the birth environment—single versus binary; isolated versus rich cluster? Are observations of debris disk systems consistent with expectations from models of planet formation (e.g., Kenyon & Bromley 2004)?

Determining why a given star has a detected disk while another apparently similar star does not has proven difficult. The clearest correlation is probably with age. A number of studies of relatively young field stars or moving group members (e.g., Rieke et al. 2005; Su et al. 2006; Rebull et al. 2008; Carpenter et al. 2009) suggest that the frequency for detection of debris disks around stars from a few solar masses to about half a solar mass is highest at age ∼10–30 Myr and then slowly declines to older ages. Why stars of similar age show diverse debris disk properties is much less clearly constrained by observations. It could be that the stars showing excesses are primarily just the ones that have had recent, large collisions in their asteroid belts producing copious amounts of small dust particles via collisional cascades (Kenyon & Bromley 2004). Alternatively, stars with strong dynamo-driven winds may scour small grains from their disks; the stars with detected IR excesses might therefore be those with comparatively weak winds (Chen et al. 2005; Plavchan et al. 2005). Debris disks might have difficulty forming in at least some types of binary systems, leading to a prediction that the stars with mid-IR excesses might preferentially be single. However, Trilling et al. (2007) obtained MIPS data for a sample of A and F binaries and concluded that, on average, binary stars (in this mass range) do not seem to have significantly different debris disk detection frequencies

* This work is based (in part) on observations made with the *Spitzer Space Telescope*, which is operated by the Jet Propulsion Laboratory, California Institute of Technology, under NASA contract 1407.
† This publication makes use of data products from the Two Micron All Sky Survey, which is a joint project of the University of Massachusetts and the Infrared Processing and Analysis Center/California Institute of Technology, funded by the National Aeronautics and Space Administration and the National Science Foundation.

compared to single stars. For binary stars that do have debris disks, the data suggested that debris disks are most frequently seen for systems with close (<3 AU) or wide companions (>50 AU).

There are two complementary paths to address many of the above issues: via observation of samples of nearby field stars and via observation of stars in open clusters. The field star path has the considerable advantage that, in general, the targets can be selected to be quite nearby, allowing smaller dust excesses to be detected and allowing the photospheres of the star to be detected at 70 μm for the nearest field stars. However, the field star sample cannot address the question of dependence on stellar environment. That is, while it is known that most stars are born in clusters and subsequently become field stars when their natal cluster is disrupted through dynamical evolution (Lada et al. 1991; Porras et al. 2003), there is no way to determine with any confidence whether a given field star was born in a rich cluster or a small group. Also, ages for field stars are very uncertain and attempting to infer how debris disk characteristics evolve with time using a field star sample is at best difficult.

The nearest open clusters offer the possibility of providing the best answers to some of the disk evolution questions. Several programs have obtained *Spitzer* MIPS data for members of the Pleiades ($t \sim 100$ Myr; $d \sim 133$ pc). From a pointed survey as part of the Formation and Evolution of Planetary Systems (FEPS; Meyer et al. 2006) Legacy program, Stauffer et al. (2005) detected small 24 μm excesses around ~4 of 20 G dwarf members. Independent of the FEPS program, Gorlova et al. (2006) obtained an MIPS scan map of the central square degree of the Pleiades, again detecting small 24 μm excesses for about 15% of the members. Finally, Sierchio et al. (2010) obtained pointed 24 μm photometry for 37 solar type Pleiades members, deriving a 32% excess frequency for cluster members of about solar mass. As a partial list, other open clusters for which MIPS data have been obtained include: IC 2391 ($t \sim 50$ Myr; $d \sim 150$ pc; Siegler et al. 2007); NGC 2547 ($t \sim 30$ Myr; $d \sim 390$ pc; Gorlova et al. 2007); NGC 2232 ($t \sim 25$ Myr; $d \sim 350$ pc; Currie et al. 2008); NGC 2451 ($t \sim 50$–80 Myr; $d \sim 200$–400 pc; Balog et al. 2009); Praesepe ($t \sim 600$ Myr; $d \sim 180$ pc; Gaspar et al. 2009); and NGC 2422 ($t \sim 100$ Myr; $d \sim 425$ pc; Gorlova et al. 2004).

Open clusters come with a wide range of initial properties—at least richness and metallicity, but potentially also the initial mass function (IMF), binary fraction or primordial disk fraction might vary from cluster to cluster. Now that open clusters have been observed spanning a wide range of ages, it would seem of interest to observe clusters that could possibly shed light on whether debris disk frequency depends in any significant way on cluster properties other than age. As noted above, the Pleiades provides a template for debris disk properties at 100 Myr for a rich, solar-metallicity, kinematically normal cluster (i.e., the space motion of the Pleiades is very similar to the space motion of the many nearby, young stars that form the Local Association). Another relatively nearby open cluster with an age of ~100 Myr is Blanco 1 (galactic latitude $\sim -79°$; ecliptic latitude $= -28°$; distance $= 250$ pc; $E(B-V) = 0.01$). As illustrated in Figures 1 and 2, Blanco 1 has some properties that make it quite dissimilar to the Pleiades. First (Figure 1), Blanco 1 is much less rich, but is particularly deficient in high mass stars—specifically, it has just two B star members (a B8 and a B9) and no member with M(V) < 0.0 versus the Pleiades having 14 B stars (and at least one white dwarf member, whose precursor was presumably an O or early B star). At very early

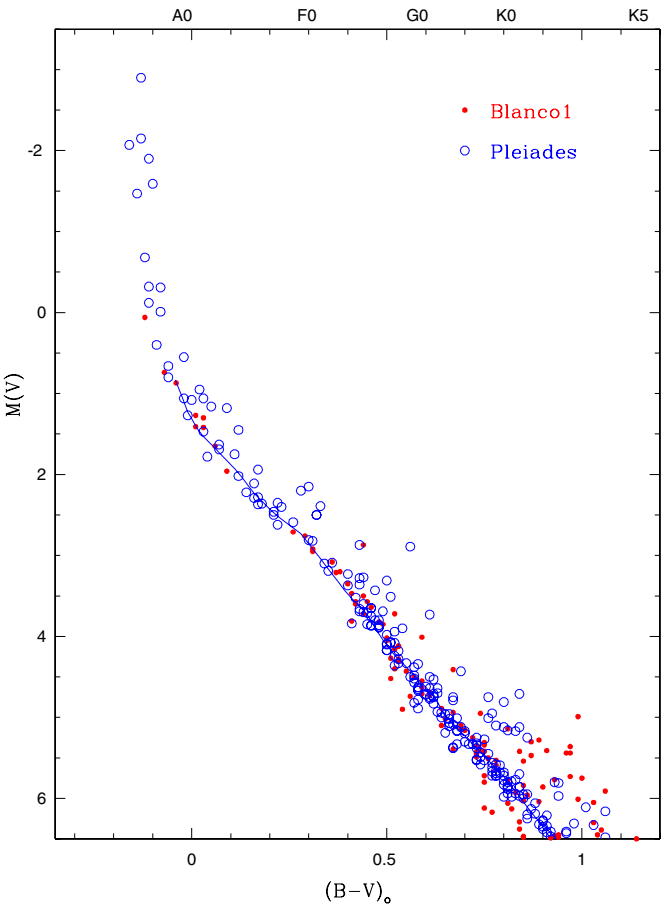

Figure 1. CMD for high mass members of the Pleiades and Blanco 1. Distances of 133 and 250 pc, and $E(B-V)$ of 0.04 and 0.01 for the Pleiades and Blanco 1, respectively, were assumed. Blanco 1 is deficient in high mass stars compared to the Pleiades.

(A color version of this figure is available in the online journal.)

ages (<a few Myr), therefore, dynamical interactions (Bate et al. 2003) or the winds and UV radiation from high mass stars (Adams et al. 2004) may have truncated the primordial disks of the low mass stars in the proto-Pleiades more than in the proto-Blanco 1 cluster. Figure 2 shows that Blanco 1 is an extreme outlier in terms of its height above the galactic plane. Either the molecular cloud from which it formed had unusual kinematics (it was a high-velocity cloud) or some external event, such as a very nearby supernova or winds from nearby O stars, imparted a significant amount of momentum to the proto-cluster when it was being formed (Oort & Spitzer 1955). Radiation driven implosion models for star formation triggered by external events in some cases predict significantly high accretion rates for protostars (Motoyama et al. 2007) or IMFs different from normal star formation events (Bertoldi 1989).

If everything involved in debris disk formation and evolution only involves the local environment of individual protostars, then one would predict no significant difference in the debris disk frequency and IR-excess sizes of Pleiades and Blanco 1 members. If the debris disk frequency in Blanco 1 were significantly different from that of the Pleiades, explanations involving the differing properties of the two clusters could be explored which might lead to a better general understanding of what controls debris disk formation and evolution. In this paper,

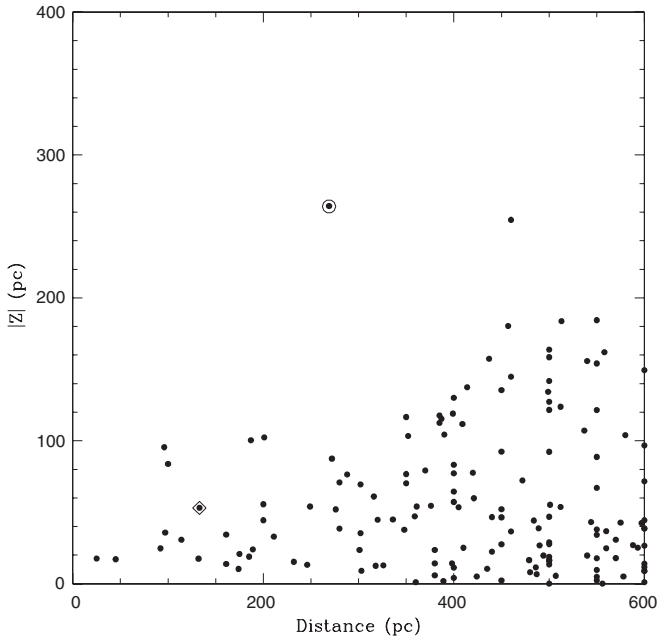

Figure 2. Height above the galactic mid-plane vs. distance for all open clusters in the Dias et al. (2002) catalog. The open circle marks Blanco 1; the diamond symbol marks the Pleiades. Blanco 1 is located further above the mid-plane than any other cluster within this distance range.

we present MIPS 24 μm data for a sample of about 40 members of Blanco 1. Our goals are to better understand (1) the disk frequency at 100 Myr; (2) how the debris disk properties of the Blanco 1 members compare to those for other similar age open clusters; and (3) to examine how debris disk presence correlates with other stellar properties such as rotation, X-ray luminosity, or binarity.

2. TARGET SELECTION AND *SPITZER* OBSERVATIONS

Based on very recent efforts, good membership lists for Blanco 1 now exist over essentially the entire stellar mass range (Moraux et al. 2007; Mermilliod et al. 2008; Cargile et al. 2009; Gonzalez & Levato 2009; D. J. James et al. 2010, in preparation). However, when the target list for this program was constructed in 2004, membership information was much spottier. The primary information available to us included several large photometric studies (Westerlund et al. 1988; Edvardsson et al. 1995), moderate resolution spectroscopy providing chromospheric diagnostics and lithium equivalent widths (Panagi et al. 1994; Panagi & ODell 1997), and X-ray imaging of the cluster to identify stars with strong coronal emission (Pillitteri et al. 2004 and references therein).

The 25 stars we selected for observation with MIPS consist of a nearly complete list of the high-probability members of the cluster known in ~2004, within the approximate spectral type range A0 to G0. All of these stars were selected as photometric and proper motion members of the cluster; most of the later-type stars also have activity indicators supporting membership.

With new membership available to us now based on modern $BVIJHK_s$ photometry, accurate radial velocities, and improved proper motions (Mermilliod et al. 2008, Gonzalez & Levato 2009), we have re-examined the membership of these stars. All of them are confirmed as high-probability cluster members in one or both of Mermilliod et al. and Gonzalez & Levato, with all of them being radial velocity members of the cluster based on multiple observations. All of them are also confirmed as cluster members from proper motion studies, and all of them are good photometric members of the cluster (see Figures 3 and 4).

Table 1
Summary of MIPS Observations of Blanco 1

Target Object	Map Center (J2000)	AORKEY
W23=ZS18	$0^h00^m55\overset{s}{.}35, -30^d03^m51\overset{s}{.}0$	17690368
W28=ZS26	$0^h01^m24\overset{s}{.}48, -30^d38^m58\overset{s}{.}3$	17690624
W35=ZS39	$0^h01^m57\overset{s}{.}75, -30^d09^m28\overset{s}{.}7$	17690880
W36	$0^h02^m04\overset{s}{.}13, -30^d41^m06\overset{s}{.}8$	17691136
W38=ZS48	$0^h02^m21\overset{s}{.}63, -30^d08^m21\overset{s}{.}6$	17691392
W51=ZS77	$0^h02^m55\overset{s}{.}23, -30^d08^m59\overset{s}{.}2$	17691648
W53=ZS84	$0^h03^m10\overset{s}{.}81, -30^d10^m48\overset{s}{.}9$	17691904
W56=ZS91	$0^h03^m20\overset{s}{.}61, -29^d49^m22\overset{s}{.}7$	17692160
W57=ZS96	$0^h03^m21\overset{s}{.}85, -30^d01^m10\overset{s}{.}5$	17696512
W58=ZS90	$0^h03^m24\overset{s}{.}39, -29^d48^m49\overset{s}{.}3$	17692416
W60=ZS101	$0^h03^m28\overset{s}{.}98, -30^d19^m27\overset{s}{.}2$	17692672
W61=ZS104	$0^h03^m31\overset{s}{.}89, -29^d43^m04\overset{s}{.}8$	17692928
W63=ZS99	$0^h03^m33\overset{s}{.}59, -30^d28^m42\overset{s}{.}0$	17693184
W68=ZS107	$0^h03^m50\overset{s}{.}17, -30^d03^m55\overset{s}{.}7$	17693440
W70=ZS110	$0^h04^m00\overset{s}{.}02, -30^d19^m15\overset{s}{.}8$	17693696
W79=ZS129	$0^h04^m31\overset{s}{.}66, -30^d14^m41\overset{s}{.}6$	17695744
W86=ZS136	$0^h04^m50\overset{s}{.}82, -29^d37^m58\overset{s}{.}9$	17693952
W88=ZS139	$0^h04^m53\overset{s}{.}33, -30^d15^m23\overset{s}{.}8$	17694208
W91=ZS138	$0^h04^m58\overset{s}{.}84, -30^d09^m41\overset{s}{.}6$	17694464
W96=ZS157	$0^h05^m26\overset{s}{.}76, -30^d17^m24\overset{s}{.}5$	17694720
W99=ZS 160	$0^h05^m30\overset{s}{.}94, -29^d53^m08\overset{s}{.}2$	17696256
W104=ZS166	$0^h05^m42\overset{s}{.}96, -29^d57^m38\overset{s}{.}2$	17694976
W113=ZS182	$0^h06^m16\overset{s}{.}35, -30^d05^m57\overset{s}{.}0$	17696000
W124=ZS199	$0^h07^m07\overset{s}{.}81, -30^d33^m41\overset{s}{.}6$	17695232
W126	$0^h08^m01\overset{s}{.}90, -30^d01^m54\overset{s}{.}1$	17695488

The targeted cluster members, their J2000 positions, and the *Spitzer* Astronomical Observation Request (AOR) identification numbers (AORKEYs) for our MIPS observations are provided in Table 1. We generally provide two identification names for our targets—the name from Westerlund et al. (1988; Wxxx) and the name from de Epstein & Epstein (1985; ZSxxx, where "ZS" stands for Zeta-Sculptor, the alternative name for the Blanco 1 cluster, derived from the brightest proposed cluster member—although Zeta Zcl is no longer considered a member of the cluster. These data were obtained under *Spitzer* program 30022.

Each target was observed using an MIPS photometry AOR at 24 and 70 μm. Our AORs are the same for all of our targets and are very similar to those used for most of the FEPS Pleiades observations. In particular, we obtain four cycles of 10 s integration time for 24 μm and seven cycles of 10 s integration time for 70 μm. We limited ourselves to seven cycles at 70 μm based on Figure 7 of Bryden et al. (2006), which showed that the confusion noise level was reached for typical galactic fields after about five cycles of 10 s integration time photometry for MIPS-70. None of the targets were detected at 70 μm, and the upper limits were deemed to be too shallow to be of use in the current study, and so we no longer discuss the 70 μm data in the present paper.

Each of our MIPS observations produced two regions of the sky covering about $6' \times 6'$ with flux densities at 24 μm—one centered on the target object and a second serendipitous field offset from that primary field by an order of $12'$. In order to attempt to expand the number of stars in our study, we also cross-correlated a master list of possible Blanco 1 cluster members against the area of the sky included within our MIPS coverage. This master list is a merger of the candidate member catalog from Panagi & O'Dell (1997) and Table 1 from Mermilliod et al.

(2008). We also incorporated membership information for the brightest cluster members from Perry et al. (1978) and from the Hipparcos proper motions (Perryman et al. 1997). Additional membership data for faint candidate cluster members came from new photometry, proper motions, radial velocities, and lithium equivalent widths reported in D. J. James et al. (2010, in preparation). Twenty additional probable Blanco 1 members, which are detected in our MIPS images, were identified. However, we were only able to derive reliable flux densities for 12 of these stars (the ones brighter than $K_s = 11$). These 12 stars are almost all fainter (and hence of lower mass) than the primary targets. Nine of these additional members are high-probability cluster members based on the Mermilliod et al. (2008) program (i.e., based on proper motions, photometry, and multiple radial velocity measurements). Of the remaining sources, ZS38 is a proper motion and photometric member but is also an X-ray source (Cargile et al. 2009) and a spectroscopic member based on radial velocity and lithium abundance (Jeffries & James 1999). ZS83 is a photometric member, a proper motion member, and an X-ray source (Cargile et al. 2009); ZS83 has a lithium abundance N(Li) = 2.3 which for its ∼K0 spectral type indicates that it is quite young (Jeffries & James 1999). The Jeffries & James radial velocity for ZS83 is a few kilometers per second off the cluster mean, which Cargile et al. (2009) take to indicate that it is an SB1. Given the combination of proper motion, X-ray detection, and youth based on lithium, we agree and conclude that ZS83 is a highly probable member of the cluster. That only leaves ZS108 as having no published, modern data supporting cluster membership. In D. J. James et al. (2010, in preparation), we show that it is also a probable cluster member, based on its photometry ($V = 13.46$; $B - V = 1.06$; $V - I_c = 1.21$), proper motion ($\mu_{\rm R.A.} = 23.4 \pm 0.5$ mas yr^{-1}; $\mu_{\rm decl.} = 3.9 \pm 0.8$ mas yr^{-1}; membership probability $P = 57\%$), and lithium abundance (EqW = 22 mÅ; N(Li) ∼ 0.6). James et al. obtained six WIYN/HYDRA spectra of ZS108, one of which showing it to be an SB2 and the others showing it to be a radial velocity variable (ranging from −20 to +40 km s^{-1}). Based on these data, we consider it to be a probable member of the cluster. A complete list of the Blanco 1 members for which we have obtained MIPS photometry is provided in Table 2.

3. MIPS PHOTOMETRY

We extracted the individual basic calibrated data files (individual flux-calibrated array images) from the *Spitzer* archive and then used the Spitzer Science Center (SSC) MOPEX package (Makovoz & Marleau 2005) to construct mosaics for each AOR. We used the default interpolation scheme and outlier rejection for MOPEX, which is discussed in Makovoz & Marleau (2005) and the online MOPEX help. We self-flattened, following the SSC recommendations using IRAF. We overlap-corrected, using the default settings in the overlap module distributed as part of MOPEX. Using the APEX-1Frame package from MOPEX, we performed PRF (Point Response Function) fitting to obtain photometry for each object at 24 μm using an empirical PRF derived from photometry mode observations of relatively bright stars in relatively high galactic latitude fields (i.e., from data as similar as possible to the Blanco 1 observations). We also obtained aperture photometry for all the cluster members, using the PHOT package in IRAF. We employed an aperture of 2 pixel radius, with the sky annulus from 7 to 11 pixels. We used an aperture correction factor of 0.716 mag derived from bright stars. We converted each image to data numbers (DN) prior to doing the aperture photometry (using the DN s^{-1} MJy^{-1} sterradian^{-1} value in the FITS headers) in order to allow the use of the photometric uncertainties calculated by the PHOT package. Brighter than [24] = 10, the two flux density determinations generally agree to within a couple percent, and the values we report are the averages (except as noted below); for fainter stars, the aperture flux densities are noisier and we report only the PRF flux densities for these stars. Based on the calibration information provided by the SSC, the flux density for zero magnitude for the MIPS 24 μm magnitude scale is 7.14 Jy.

For the stars that were our original targets, each star is centered on the 24 μm array field of view (FOV), with each star falling on or near the same pixels and being observed with the standard MIPS photometry mode AOR. This is the same observing pattern as used for the MIPS calibration stars. Therefore, compared to stars that fall in other parts of the MIPS FOV (or compared to stars observed in MIPS scan map mode) some possible sources of error in the photometry are eliminated/avoided. For MIPS calibration stars with essentially arbitrarily large intrinsic S/N, repeat observations show an rms scatter in the measured 24 μm flux densities of order 0.5%–0.7%, showing that the MIPS 24 μm camera is stable enough to deliver 1% photometry if the target star is bright enough (Engelbracht et al. 2007). The sensitivity prediction tool for MIPS predicts signal-to-noise ratio (S/N) > 100 for our brightest targets and S/N of a few percent for our faintest, targeted stars. The uncertainty estimates returned by PHOT agree with these expectations, and we report these uncertainties (for our original target stars) as the parenthetical numbers following the 24 μm magnitudes in Table 2.

For the serendipitous Blanco 1 members reported in Table 2, other sources of error may affect the photometry (flat field errors; array location dependent point-spread function or filter response corrections). Rather than adopting the uncertainties for each star reported by APEX or PHOT, we have chosen to determine empirical uncertainty estimates for stars of a given flux density using regions of the sky where we have overlapping MIPS coverage (i.e., where the mosaics from two or more AORs overlap). We have two or more observations for more than 100 point sources which we sorted by flux density and grouped into several flux density bins. Within each group, we calculated the mean absolute difference for the two measures; we converted the mean absolute difference to an estimate of the error (σ) using the standard formula ($\sigma = 1.2\times$MAD). The derived 1σ values range from 4% for our brightest members to about 10% at $K_s = 11$. We report these uncertainties in Table 2 for the serendipitous cluster members (the last 12 stars in the table).

Two of the original target stars (W58 and W60) have "companions" within 2 or 3 pixels in the MIPS-24 images of comparable (though fainter) magnitude. Neither companion is visible in Two Micron All Sky Survey (2MASS) images, making it likely that these are IR-bright galaxies. The aperture photometry for these stars is compromised by the proximity of the companion object. We therefore report the PRF-fitting magnitude for these sources.

Table 2 provides data for the entire set of cluster members for which we have obtained MIPS-24 flux densities. Figures 3 and 4 show color–magnitude diagrams (CMD) using $B - V$ and $V - K_s$ as the abscissa for our entire catalog of candidate cluster members, with the stars observed with *Spitzer* highlighted (circles for our original targets; squares for the fainter, serendipitous members). The primary reference for membership in the cluster for each star is indicated by the first reference given in the rightmost column of Table 2. If only one reference is given,

Table 2
Blanco 1 MIPS and Ancillary Data

Star Name[a]	R.A. (2000) (degrees)	Decl. (2000) (degrees)	V	$B-V$	K_s	[24]	$K_s-[24]$	$v \sin i$ (km s^{-1})	$\log(L_X)$ (erg s^{-1} cm^{-2} Hz^{-1})	$\log(L_X/L_{bol})$	Comments[c]
W23 = ZS18*	0.230577	−30.064169	8.39	0.04	8.355	7.64(0.01)	0.71	...	...	...	G09; NS
W28 = ZS26*	0.351998	−30.649542	10.50	0.40	9.484	9.20(0.02)	0.28	9.0	...	...	M08
W35 = ZS39*	0.490606	−30.157967	9.96	0.32	9.158	8.87(0.02)	0.27	54.5	28.96P	−5.3	G09; P78
W36 = M901	0.517190	−30.685226	8.98	0.10	8.715	8.71(0.01)	−0.01	...	...	...	G09; P78
W38 = ZS48*	0.590125	−30.139343	10.72	0.48	9.601	9.43(0.03)	0.16	69.0	29.87C	−4.10	M08
W51 = ZS77	0.730105	−30.149778	8.43	0.02	8.427	8.48(0.01)	−0.05	...	<28.43P	−6.3	G09; P78; NS
W53 = ZS84*	0.795057	−30.180246	11.32	0.56	9.967	9.79(0.04)	0.18	24.0	29.60C	−4.2	M08
W56 = ZS91	0.835889	−29.822985	11.30	0.57	9.961	9.97(0.05)	0.00	12.8	29.43C	−4.3	M08
W57 = ZS96	0.841037	−30.019594	10.38	0.42	9.271	9.30(0.02)	−0.03	21.8	29.50C	−4.6	M08; SB
W58 = ZS90	0.851605	−29.813707	10.62	0.50	9.462	9.41(0.02)	0.01	66.0	29.65C	−4.4	M08
W60 = ZS101	0.870738	−30.324226	10.61	0.44	9.553	9.42(0.03)	0.13	19.1	...	...	M08
W61 = ZS104	0.882868	−29.718004	10.05	0.36	9.127	9.02(0.02)	0.11	...	29.75C	−4.5	G09; C09
W63 = ZS99	0.889975	−30.478338	10.62	0.45	9.498	9.46(0.02)	0.04	6.0	...	...	M08
W68 = ZS107	0.959037	−30.065468	11.04	0.54	9.844	9.77(0.03)	0.07	11.5	28.95C	−4.9	M08; SB2
W70 = ZS110	1.000072	−30.321060	11.12	0.56	9.764	9.75(0.04)	−0.03	15.7	...	...	M08; SB
W79 = ZS129	1.131912	−30.244907	11.68	0.61	10.232	10.15(0.05)	0.08	7.1	<29.59M	<−3.9	M08
W86 = ZS136	1.211755	−29.633030	8.29	0.01	8.273	8.31(0.01)	−0.05	...	...	...	G09; P78; NS
W88 = ZS139*	1.222222	−30.256613	8.32	0.05	8.271	8.07(0.01)	0.20	...	<29.32M	<−5.5	G09; P78; NS
W91 = ZS138*	1.245159	−30.161558	11.47	0.58	10.082	9.72(0.03)	0.36	18.3	29.34C	−4.3	M08
W96 = ZS157	1.361498	−30.290138	9.73	0.27	9.072	9.01(0.02)	0.06	41.5	<29.22M	<−5.1	G09; P78
W99 = ZS160*	1.378900	−29.885614	11.26	0.55	9.993	9.55(0.03)	0.44	15.3	<29.30M	<−4.4	M08
W104 = ZS166	1.429001	−29.960606	9.92	0.32	9.122	9.08(0.02)	0.03	<10	<28.99M	<−5.3	G09; P78
W113 = ZS182	1.568121	−30.099182	11.72	0.63	10.249	10.14(0.05)	0.10	8.0	29.27C	−4.3	M08
W124 = ZS199	1.782528	−30.561554	8.67	0.09	8.538	8.53(0.01)	0.00	...	...		G09; P78; NS
W126 = ZS226	2.007917	−30.031666	9.78	0.31	9.038	9.04(0.02)	−0.01	...	...		G09; P78; NS
ZS38[b]	0.476847	−30.128284	13.86	1.03	10.932	10.80(0.09)	0.13	69.1	29.82C	−3.1	J99; C09; SB2
ZS54[b]	0.617458	−30.078751	13.03	1.00	10.510	10.40(0.08)	0.11	13.5	29.69C	−3.5	M08; VB
ZS62[b]	0.647750	−30.117222	12.56	0.77	10.561	10.55(0.09)	0.01	5.0	29.40C	−3.9	M08; SB
ZS83[b]	0.779556	−30.254759	12.51	0.85	10.380	10.49(0.09)	−0.11	6.8	29.36C	−4.0	C09
ZS95[b]	0.818703	−29.979839	12.42	0.92	10.266	10.34(0.08)	0.00	10.2	28.92C	−4.5	M08
ZS100[b]	0.863876	−30.446903	12.55	0.79	10.507	10.44(0.09)	0.07	12.7	...	...	M08; SB
ZS102[b]	0.890083	−30.262501	12.50	0.77	10.729	10.57(0.09)	0.19	7.4	...	...	M08
ZS108[b]	0.977224	−30.283806	13.41	1.06	10.747	10.72(0.09)	0.03	...	...	...	J10; SB2
ZS161[b]	1.361920	−29.855742	12.67	0.79	10.754	10.75(0.09)	0.00	4.0	<29.43M	<−3.7	M08
ZS165[b]	1.398048	−29.951780	12.49	0.88	10.260	10.16(0.08)	0.10	5.0	29.41C	−3.9	M08; SB
W89[b]	1.244333	−29.563276	11.55	0.59	10.094	10.14(0.08)	−0.04	19.0	...	...	M08
M348[b]	0.854329	−30.435089	11.97	0.75	10.080	10.16(0.08)	−0.08	0.5	...	...	M08; SB

Notes.
[a] The stars with an asterisk (*) after their name have 24 μm excesses, probably due to their having debris disks, according to our analysis.
[b] Serendipitously imaged member.
[c] C09: Cargile et al. 2009; G09: Gonzalez & Levato 2009; J99: Jeffries & James 1999; J10: D. J. James et al. (2010, in preparation); M08: Mermilliod et al. 2008; P78: Perry et al. 1978.

that reference is also the source for optical photometry. If other references are given, they provide the V and $B-V$ ("NS" refers to NStED—the NASA Stellar and Exoplanet Database; for the Blanco 1 stars, the NStED V and $B-V$ photometry come from Tycho-2, where the native Tycho photometry have been converted to Johnson B and V using a formula from Bessell 2000). The K_s photometry is from the 2MASS point source catalog (Skrutskie et al. 2006). The spectroscopic rotational velocities are nearly all from Mermilliod et al. (2008); exceptions are those for ZS38 and ZS102 from Jeffries & James (1999) and those for W35, W96, W104, and ZS83 from D. J. James et al. (2010, in preparation). The rightmost column of the table also identifies stars whose binarity have been empirically detected via radial velocity variability (SB or SB2) or as a close visual pair (VB); these identifications come from Mermilliod et al. (2008) except for ZS38 and ZS108 which are attributed to D. J. James et al. (2010, in preparation).

The X-ray luminosities in Table 2 come from Micela et al. (1999), Pillitteri et al. (2003, 2004), and Cargile et al. (2009). Because it is the most recent reference, we give preference to the values provided by Cargile et al. The letters following L_X in the table point to the source of the X-ray data. Where only X-ray luminosity was provided, we have calculated $\log(L_X/L_{bol})$ ourselves, using bolometric luminosities provided by Schmidt-Kaler (1982). The literature values for L_X were calculated using slightly different assumptions (distance of 240 or 250 pc; $E(B-V) = 0.016$ or 0.02), we have ignored those small differences.

Our sample of Blanco 1 stars with MIPS photometry extends over the spectral type range from A0 to about mid-K.

4. USE OF *SPITZER* PHOTOMETRY OF THE HYADES TO CALIBRATE THE PHOTOSPHERIC $K_s-[24]$ COLOR OF LOW MASS STARS

Following the path forged by several other groups (e.g., Rebull et al. 2008 and references therein), as the measure of IR excess for the Blanco 1 cluster stars, we will use the

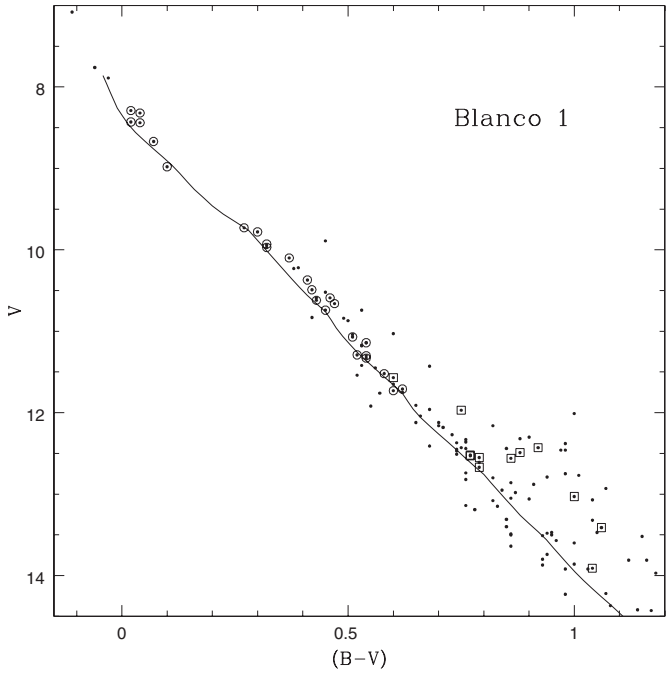

Figure 3. CMD for stars in our Blanco 1 master catalog and the stars for which we have obtained MIPS photometry. The curved line is a fit to the Pleiades single-star main sequence locus, as provided in Stauffer et al. (2007). We have assumed distances of 133 and 250 pc, and $E(B-V)$ of 0.04 and 0.01 for the Pleiades and Blanco 1, respectively. The stars we targeted in Blanco 1 are shown with circles; the additional members that happen to fall within the area covered by our MIPS mosaics are shown as open squares.

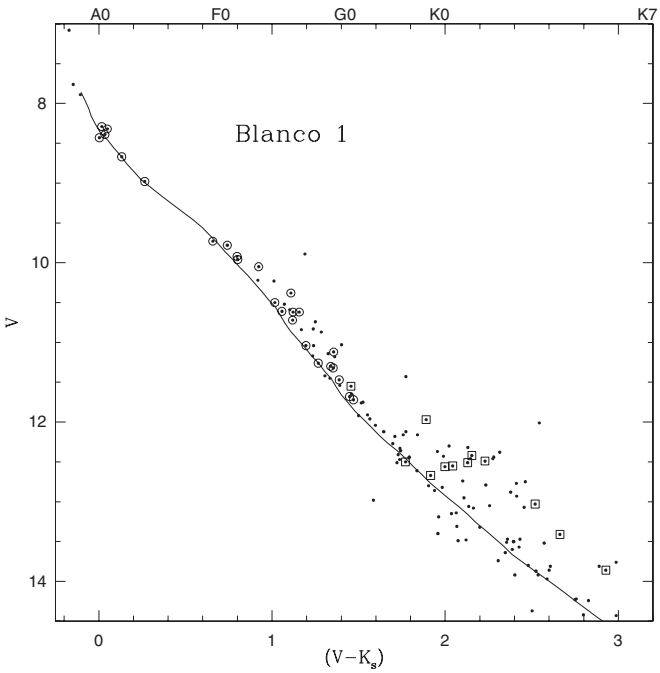

Figure 4. As for Figure 3, except using $V - K_s$ as the abscissa.

$K_s - [24]$ color, rather than fitting a photospheric model to the shorter wavelength photometry and comparing the measured 24 μm flux density to the predicted photospheric flux density. We believe that this type of analysis can, in fact, provide more sensitive detection limits for debris disks than spectral energy distribution (SED) analysis because it introduces the fewest possible assumptions and model dependencies. Also, the fact that the 2MASS catalog provides homogenous, sensitive K_s-band photometry over the entire sky insures that our measured IR-excess parameter can be placed on a common system with other stellar samples to high accuracy. However, in order to obtain the most benefit from using this method, it is necessary to have a good calibration of the photospheric colors in this plane.

For early type stars, $K_s - [24]$ color is essentially zero, making it easy to identify stars with excesses. However, as demonstrated by Gautier et al. (2007), the photospheric $K_s - [24]$ departs from zero as one goes to later spectral types, reaching values of several tenths of a magnitude at early M spectral type. Gorlova et al. (2007) derived a calibration of the trend of $K_s - [24]$ color with $V - K_s$ based on members of the Pleiades which is valid for the mass range of our Blanco 1 sample. However, the Pleiades is relatively far away and nebular emission adds structured noise, resulting perhaps in a less well-defined relation than desirable. We decided to investigate whether the *Spitzer* archive provides a better, empirical means to define the photospheric $K_s - [24]$ color for low mass stars.

After some experimentation, we believe that *Spitzer* observations for the Hyades provide the best data set to define the photospheric $K_s - [24]$ relation. The Hyades has been well observed by *Spitzer*, it is the closest open cluster (and hence has the best S/N), and the data exist for essentially the entire spectral type range for which we have Blanco 1 observations. The *Spitzer* observations of the Hyades were obtained as part of two programs—PID 148 (Carpenter et al. 2008) and PID 3371 (Cieza et al. 2008). Except where mentioned, we have simply used the *Spitzer* flux densities published in those papers. Both papers used the same flux density for zero magnitude for MIPS 24 μm as we have, and both adopted K_s magnitudes from 2MASS. Figure 5 shows how the $K_s - [24]$ color varies with the $V - K_s$ color over the spectral type range from G0 to M0. The solid curve is our fit to these data corresponding to

$$K_s - [24] = +0.042 - 0.053 \times (V - K_s) + 0.023 \times (V - K_s)^2. \quad (1)$$

The dashed curves are the 3σ bounds around the fiducial curve, where we have calculated a running estimate of the rms by ordering the stars by their $V - K_s$ color and determining the rms for each group of 10 successive stars. The 3σ bound ranges from about 0.06 mag at $V - K_s = 1.5$ to about 0.10 mag at $V - K_s = 3.0$. We exclude one observed star from this plot—HD 242780—because we discovered that it had been observed two hours after an MIPS 24 μm observation of Mon R2 which badly saturated the array and left it in an unstable state at the time of the HD 242780 observation. Another star, HD 30505, appeared to have a 24 μm excess using the published photometry from Cieza et al. (2008). However, our own flux density measurement is about 10% fainter than the published value and quite consistent with other Hyades stars of the same spectral type; we plot our flux density for this star. Our flux densities for a sample of a half dozen other stars from Cieza et al. agree with their values within the expected uncertainties; also, the Cieza et al. and Carpenter et al. stars show no significant systematic differences in their location in Figure 5.

Also shown for reference in Figure 5 are the Gorlova et al. (2007) and Plavchan et al. (2009) predictions for the photospheric $K_s - [24]$ color, where for the Plavchan et al. relation we have converted $T_{\rm eff}$ to $V - K$ using the color-temperature data in Kenyon & Hartmann (1995). Our relation differs only slightly from the Gorlova et al. predictions over the

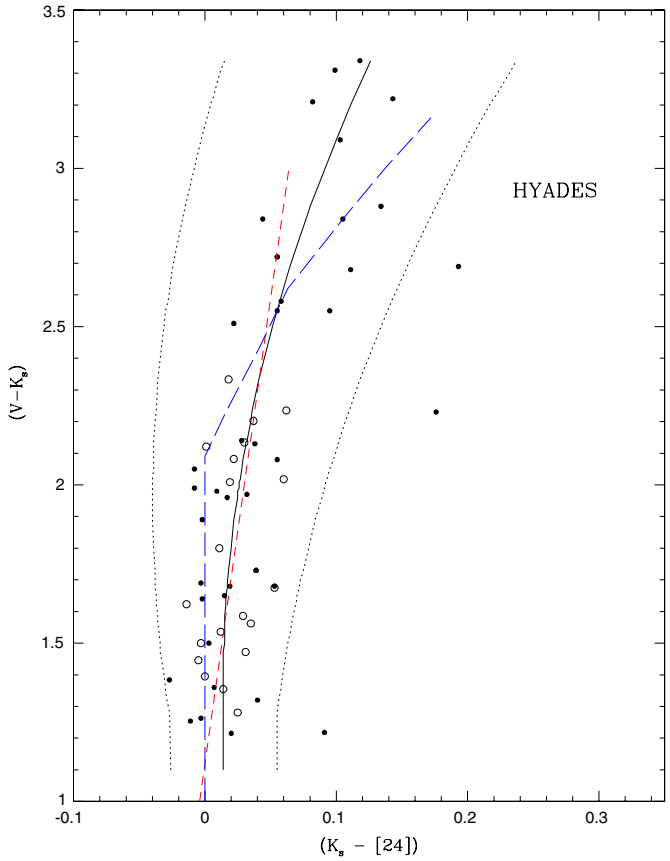

Figure 5. MIPS-24 photometry for members of the Hyades, illustrating how the photospheric $K_s - [24]$ color becomes redder for late type dwarfs. The solid curve is a fit to these data, excluding the three apparent outliers. Open circles are from PID148 and filled circles are from PID3771. The red, dashed line is the relation from Gorlova et al. (2007); the blue, dashed line is Plavchan et al. (2009) relation—see the text for details.

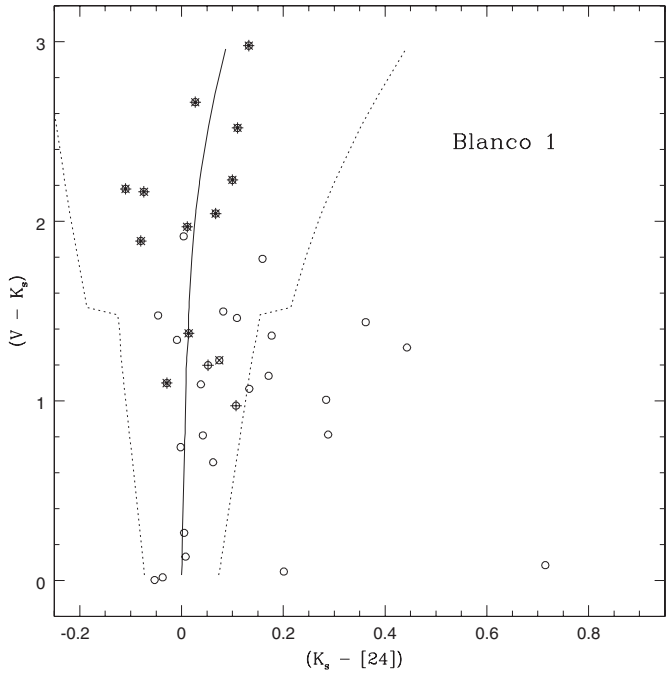

Figure 6. MIPS-24 photometry for members of Blanco 1. The solid curve is the expected photospheric relation as derived from the Hyades low mass stars, as shown in the previous figure. The dashed curves are the 3σ limits around this curve, as discussed in the text. Objects identified as spectroscopic or visual binaries are overplotted with a cross; objects identified as photometric binaries are overplotted with a plus sign; and objects identified by both techniques then appear as the combination of symbols.

range of validity of the two relations. We differ more from the Plavchan et al. relation, particularly at the red end. The bluest field M dwarfs of Gautier et al. (2007) have $K_s - [24] \simeq 0.35$ at $V - K_s = 4$. The Plavchan et al. relation is designed to link smoothly to the field M dwarfs; our Hyades relation would have to steepen significantly just redward of our faintest stars to be consistent with the Gautier et al. data. For the purposes of this current paper where all of the objects of interest have $V - K_s < 3$, we believe that the Hyades relationship provides the best available means to predict the photospheric $K_s - [24]$ color.

There are three Hyades members that fall outside the 3σ upper limit shown in Figure 5: they are vB 19 (HD 26784), VA 133 (HDE 285690), and VA 407 (HDE 286789)—all from PID 3771. We have made our own measurement of the 24 μm flux density for these three stars. Our flux densities are about 3% fainter than the published ones for VA 133 and VA 407, but even using our values these objects' $K_s - [24]$ colors fall above the 3σ curve. Our flux density for vB 19 is essentially the same as the published value. We see no evidence in the MIPS nor 2MASS images for any source confusion. Cieza et al. (2008) did not identify these stars (or any other low mass Hyades member) as debris disk candidates. Their method to identify excesses was to use NextGen (Hauschildt et al. 1999) model atmosphere predictions of the IR SEDs, using published spectral types of the Hyades stars to select which model to use and normalizing the model spectra to their 2MASS photometry. Because our color-based technique for estimating excesses is internally self-calibrating (the majority of the stars define the locus of non-excess objects) and has fewer additional input parameters (each of which may introduce further uncertainties), we believe that our technique is capable of detecting smaller excesses and that these three stars have small IR excesses.

5. IDENTIFICATION OF BLANCO 1 MEMBERS WITH APPARENT 24 μm EXCESSES AND THE PHYSICAL INTERPRETATION OF THOSE EXCESSES

5.1. Blanco 1 Members with Excesses

Figure 6 shows a plot of the $K_s - [24]$ color versus K_s magnitude for the members of Blanco 1 for which we have MIPS observations. The solid curve is the relation derived from the Hyades stars (for $V - K_s > 1.2$); for $V - K_s < 1.2$, we simply extrapolate this relation to $V - K_s = 0.0$ where we adopt $K_s - [24] = 0.00$ at that color. The Blanco 1 3σ curves are based on our estimated 24 μm flux density uncertainties as described in Section 3. Specifically, for $K_s < 10$, we adopt 1σ $K_s - [24]$ uncertainties ranging from 0.02 at $K_s = 8$ to 0.045 at $K_s = 10$; for the fainter stars, the adopted 1σ $K_s - [24]$ uncertainties range from 0.07 at $K_s = 10$ to 0.10 at $K_s = 11$.

Eight stars fall well to the right of the 3σ upper limit curve in Figure 6. They are W23 (A0V), W28 (F5), W35 (A9/F0), W38 (∼F5), W53 (∼G0), W88 (A0V), W91 (∼G0), and W99 (∼F8). W60 ($V - K_s \sim 1.06$, $K_s = 0.13$) falls just slightly above the 3σ limit; however, we do not include it as a detected excess star because it is one of the two cluster members with nearby sources contaminating the MIPS photometry (see previous section), thus making its photometry more uncertain. Assuming that all eight of the stars with 24 μm excesses have debris disks, the derived disk frequency for our sample of A0 through M0 Blanco 1 stars is 8/37 or about (22 ± 8)%. However, because our [24]

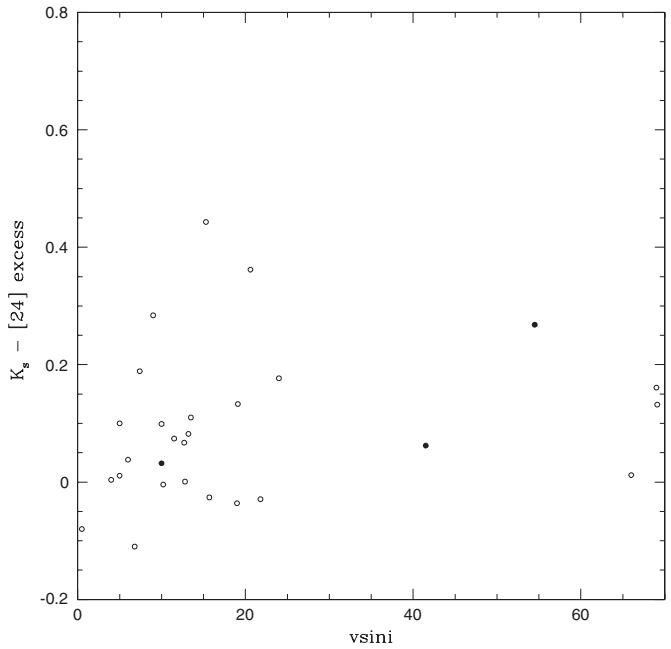

Figure 7. $K_s - [24]$ color vs. spectroscopic rotational velocity for members of Blanco 1 for which we have MIPS data. Filled dots are early type stars with $B - V < 0.35$ (corresponding to spectral type earlier than about F3), which have no outer convective envelope and hence for which there is no expectation for a wind.

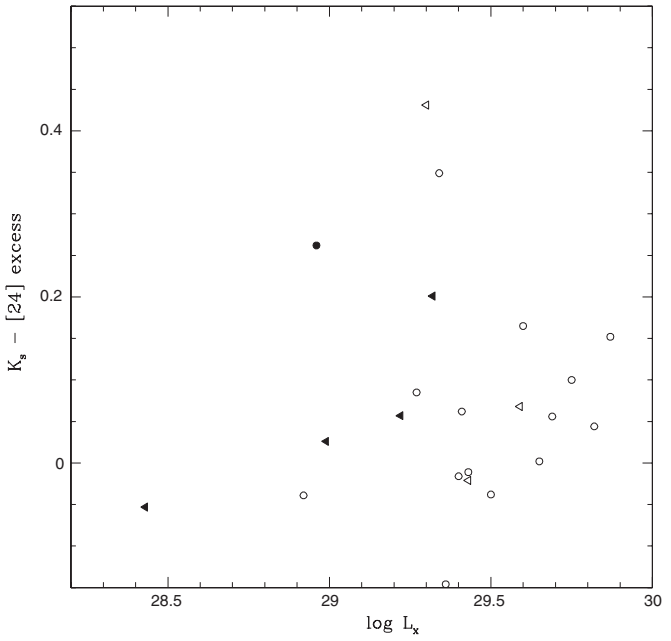

Figure 8. $K_s - [24]$ color vs. Log (L_X) for members of Blanco 1 for which we have MIPS data. Filled symbols are stars with $B - V < 0.35$, not expected to be strong X-ray sources (or to have strong winds) because they lack outer convective envelopes. Leftward pointing triangles are X-ray upper limits.

uncertainties are relatively large for the fainter, serendipitous members, if we restrict ourselves to just the original set of targeted cluster members where our uncertainties allow us to detect 3σ excesses of 0.15 mag or larger, our detection frequency is 8 of 25, or $(32 \pm 11)\%$. This is comparable to the 30%–45% detection frequency for NGC 2547 B–F stars found by Gorlova et al. (2007) and the $(32 \pm 7)\%$ detection frequency for late F to early K dwarf members of the Pleiades by Sierchio et al. (2010). If one restricts the comparison to just the Pleiades and NGC 2547 stars in about the same mass range as the Blanco 1 stars (see Section 6 and the Appendix), the Pleiades and NGC 2547 disk fractions are $(21 \pm 4)\%$ and $(41 \pm 7)\%$, respectively.

5.2. Active Galactic Nucleus Contamination?

Both active galaxies (Seyferts and QSOs) and star-forming galaxies are bright at 24 μm. The surface density of extragalactic sources increases rapidly at fainter flux densities (Papovich et al. 2004). As one attempts to detect debris disks around progressively lower mass members of open clusters, the probability that the line of sight to a given cluster member intersects a comparably bright distant galaxy increases. Fainter than [24] = 11 (corresponding to 24 μm flux density $\sim$0.3 mJy), the chance that a 15% flux density excess is due to a random line-of-sight contamination by an extragalactic source becomes quite significant. That was one reason we chose not to report 24 μm photometry for the faintest detected sources in Blanco 1. One can use the source counts in Papovich et al. (2004) to estimate the probability that any of our reported debris disk candidates are false positives due to extragalactic contamination. We adopt the same assumptions for our contamination estimates as in Gaspar et al. (2009) for their analysis of *Spitzer* MIPS observations of Praesepe. Specifically, we adopt a matching radius for chance alignment of 3.″6 and a minimum flux density excess of 15% of the photospheric flux density. For our seven brightest cluster members ($7.5 < [24] < 9$), the surface density of sufficiently bright extragalactic sources is relatively low, and the probability that any of these sources has a 24 μm excess to line-of-sight contamination is small (<5%). However, given the total number of targets in our sample with $9 < [24] < 11$, one would expect more than a 50% chance of finding one falsely identified 24 μm excess source (vs. the five objects in this mass range that we actually identify as having excesses). In the event of such a contaminant, in most cases the galaxy would not be *exactly* aligned with the Blanco 1 member, and the resultant 24 μm centroid would be displaced from the true Blanco 1 stellar position (as defined by the position derived from the 2MASS data). Our debris disk candidates show no such positional offsets, and we therefore prefer to accept all six as having real 24 μm excesses.

5.3. Correlation of IR-excess and Other Stellar Parameters

There is a theoretical expectation that winds could scour disks of small particles (Chen et al. 2005; Plavchan et al. 2009), and therefore one might expect a correlation between the 24 μm excess and a wind proxy. Figures 7, 8, and 9 provide several means to possibly identify such a correlation. Stellar rotation (or more specifically differential rotation) drives the dynamo activity that is thought to power winds from low mass stars with outer convective envelopes. The wind mass loss rate is thought to saturate above some rotational velocity, so one probably does not expect a linear dependence on rotation—but at least stars with rotational velocities less than 10–20 km s^{-1} should have comparatively weak winds. Instead, Figure 7 shows basically no correlation between rotation and IR excess. The quiescent X-ray emission of late-type stars arises from non-thermal heating of the stellar corona, again driven by dynamo activity whose ultimate source is differential rotation in the outer convective envelope. Above some critical rotational velocity, $\log(L_X/L_{bol})$ becomes saturated. It is not known if the wind mass loss rate becomes saturated at the same critical rotational velocity, but that is a plausible assumption. If so, then one

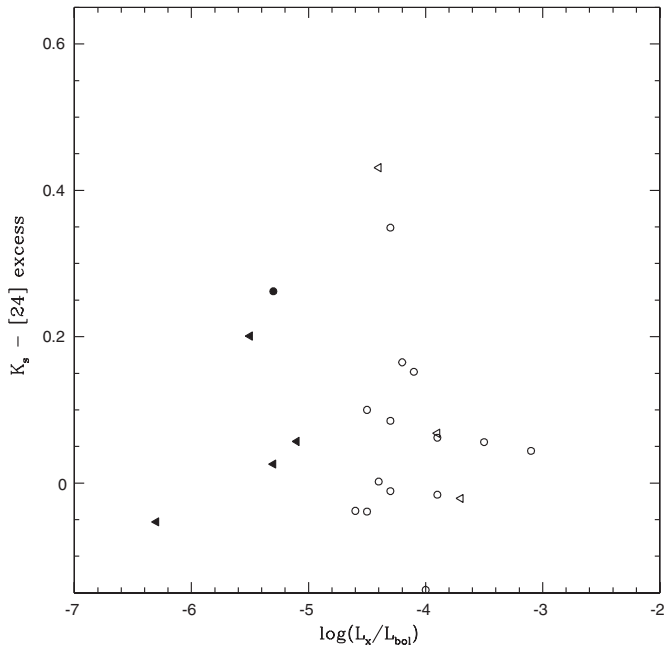

Figure 9. $K_s - [24]$ color vs. Log (L_X/L_{bol}) for members of Blanco 1 for which we have MIPS data. Filled symbols are stars with $B - V < 0.35$. Leftward pointing triangles are X-ray upper limits.

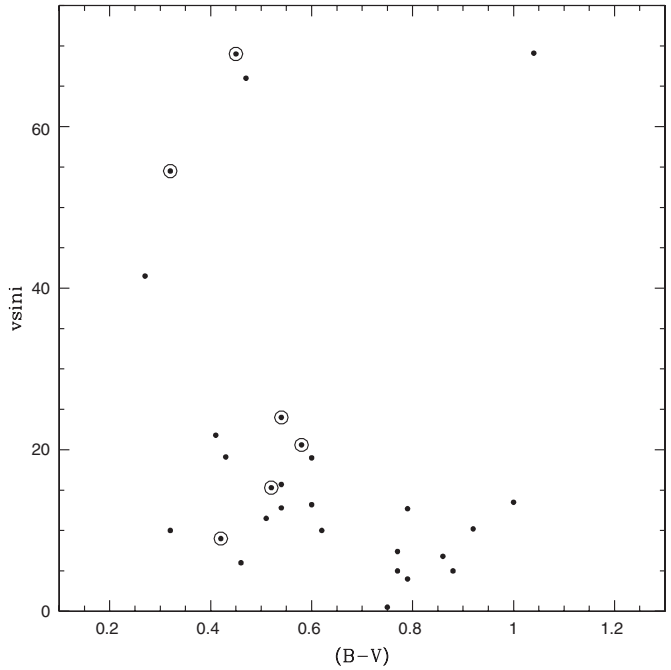

Figure 10. Rotational velocities for Blanco 1 members for which we have MIPS data. The encircled dots are stars with apparent 24 μm excesses.

would expect the largest excesses for stars with weak X-ray emission and either no excesses or smaller excesses for stars with saturated X-ray emission. Figures 8 and 9 instead show essentially no correlation in the expected sense. At face value, this would seem to argue against the wind scouring model; however, as noted in the next paragraph, that conclusion is probably unwarranted.

In Figure 7, we have shown that there is no strong correlation between rotation and 24 μm excess for our Blanco 1 F, G, and K dwarfs. Is that plot indicative that there truly is no dependence of mid-IR excess on stellar rotation at this epoch? We believe that the answer to that question is "no" because the stars in our sample of Blanco 1 members are not well suited to testing this hypothesis. This is illustrated in Figure 10, a plot of $v \sin i$ as a function of $B - V$ for the Blanco 1 stars for which we have MIPS data and rotational velocity measures. The six stars for which we have both types of data and which have 24 μm excesses are marked with open circles. The plot shows that while there is a range in rotational velocity for the Blanco 1 targets, that range mostly just reflects the expected dependence of rotation on mass (early F stars are rapid rotators; late F stars and G dwarfs are slow rotators)—and at a given mass there is not much spread in rotation. The stars with 24 μm excesses have rotational velocities typical for their mass. Our sample of stars could not provide a strong test of the dependence of debris disk presence on rotation for stars with outer convective envelopes because of this. The only star in our sample which could provide some degree of a test is ZS38—the rapidly rotating K dwarf with $B - V = 1.04$ and $v \sin i = 69$ km s^{-1}. If it had been found to have a 24 μm excess, that would have been at odds with the expectation that a star expected to have a strong dynamo wind should have scoured its disk. One star does not provide a good statistical test.

The best empirical linkage between presence of a 24 μm excess and another observable which we have been able to identify in our data is a correlation with a proxy for multiplicity—specifically, with displacement above the single-star main sequence

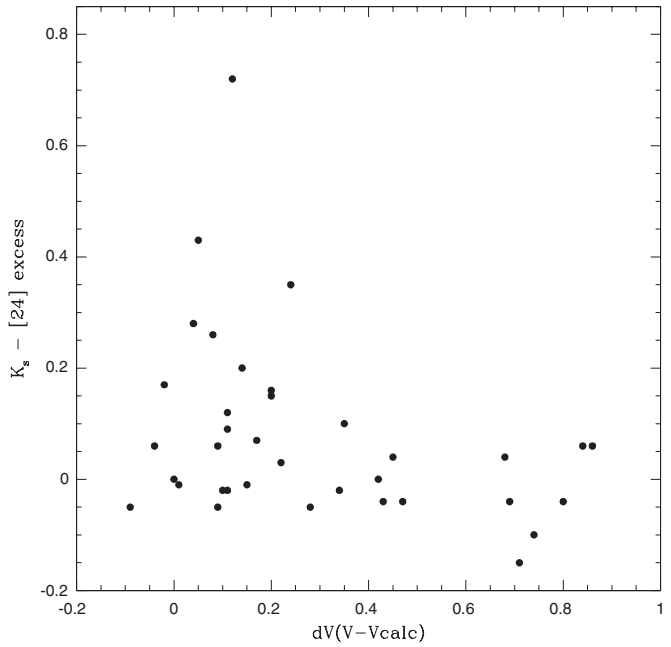

Figure 11. $K_s - [24]$ excess vs. the height above a single-star main sequence curve for members of Blanco 1 for which we have MIPS data. The stars plotted have inferred spectral types from about A0 to mid-K.

in a CMD. Figure 11 shows this dependency. The displacement above the main sequence has been calculated relative to the Pleiades single-star main sequence shown in Figure 4, shifted to Blanco 1 distance. Identifying photometric binaries as those stars with displacements above the single-star main sequence more than 0.3 mag, a two-sample Kolmogorov–Smirnov test yields just a 6% chance that the single and binary stars in Figure 11 have $K_s - [24]$ excess distributions drawn from the same parent distribution. We discuss this possible dependence of excess frequency on binarity in more detail in the next section.

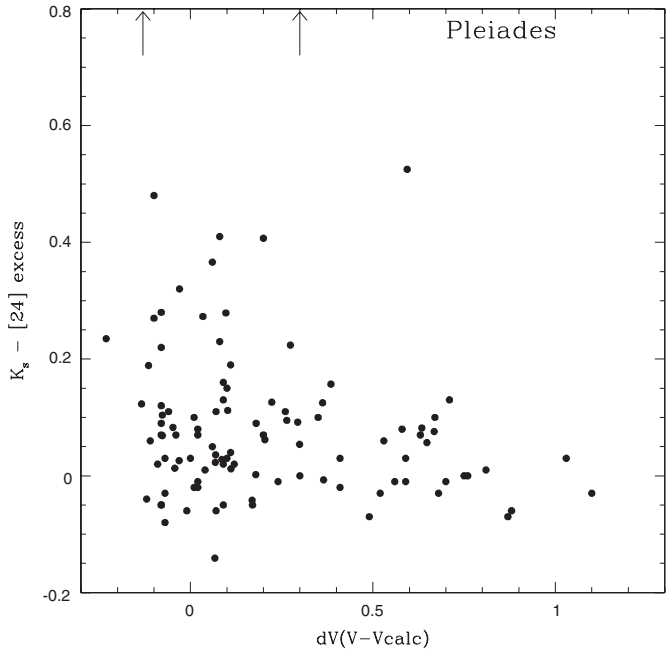

Figure 12. K_s − [24] excess vs. the height above a single-star main sequence curve for members of the Pleiades with MIPS data. Arrows point to the location of two stars that are off-scale—HII1132 and AKII437.

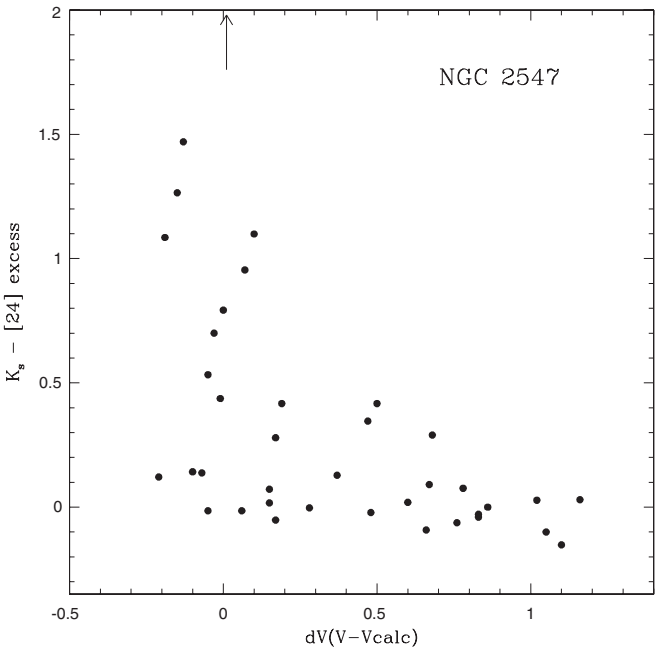

Figure 13. K_s − [24] excess vs. the height above a single-star main sequence curve for A0 to mid-K members of NGC 2547 with MIPS data. The arrow points to the location of one star that is off-scale—ID8 (see Table 5 of Gorlova et al. 2007).

6. THE CORRELATION BETWEEN 24 μm EXCESS AND BINARITY IN OTHER OPEN CLUSTERS

As noted in the preceding section, the strongest linkage between 24 μm excess and any other stellar property is with a binarity proxy. Interpretation of that dependency is made more complicated, however, by the nature of our Blanco 1 object sample. As shown in Figures 4 and 6, all of our stars with probable 24 μm excess have $V - K_s < 1.5$, whereas most of our stars that are photometric binaries have $V - K_s > 1.5$. Therefore, the apparent link between 24 μm excess and displacement above the single star sequence could arise if lower mass stars in Blanco 1 had much lower probability of having a detectable 24 μm excess. A correlation between detected 24 μm excess and mass has been noted in some studies (e.g., Siegler et al. 2007; Gaspar et al. 2009). In particular, Figure 6 of Siegler et al. indicated a three times higher 24 μm excess frequency for B and A stars compared to FGK dwarfs at the age of the Pleiades (i.e., the age of Blanco 1). Given the small number of stars in our sample, this could explain most of the correlation we see in Figure 11.

A test as to whether the apparent link between 24 μm excess and binarity is the result of peculiarities in our sample selection or is a real effect is to look for a similar correlation in other open cluster data sets. This is more difficult than it would appear because (1) one needs a relatively young and rich cluster, so that there are a significant number of stars with excesses; (2) the cluster needs to have good membership information and good optical/near-IR photometry; and (3) the MIPS data must be sensitive enough to detect a large sample of cluster members (preferably covering the spectral type range we have sampled in Blanco 1). We believe that the two clusters that have the best data to make this test are the Pleiades (age $\sim$ 100 Myr) and NGC 2547 (age $\sim$ 30 Myr; Jeffries & Oliveira 2005).

For this test, we limit the sample of Pleiades and NGC 2547 stars to those with $0.0 < V - K_s < 3.0$ for several reasons: (1) to approximately match the mass range of the Blanco 1 sample; (2) to avoid B stars, since young B stars can have IR excesses from physical causes other than debris disks (Gorlova et al. 2006; 2007); (3) because the main-sequence slope in V versus $V - K_s$ becomes so steep for $V - K_s < 0.0$ that it becomes very difficult to determine useful displacements above the main sequence in order to identify binary stars; and (4) because B stars can be displaced above the main sequence because they are post-main sequence—also making it impossible to use their location in a CMD to identify binaries. More details of the sample of stars in each cluster, their K_s − [24] colors, and their displacements above a single star main sequence can be found in the Appendix.

Figures 12 and 13 provide the plots of K_s − [24] excess versus height above the main sequence for the Pleiades and NGC 2547. Both plots show the same dependency as found for Blanco 1, with the photometric binary stars having a much lower frequency of 24 μm excesses compared to the stars that lie near the single-star main sequence. As for Blanco 1, we use a height above the main sequence of 0.3 mag to separate "single" and binary members of the clusters. A two-sample KS test yields just a 2% chance that the single and binary stars in NGC 2547 have K_s − [24] excess distributions drawn from the same parent distribution; for the Pleiades, the KS test returns a 13% probability. Combining all of the single and binary stars for all three clusters together, the KS test yields a 0.05% chance that the single and binary stars are drawn from the same parent distribution. Additional discussion of the correlation between binarity and debris disk detection can be found in Sierchio et al. (2010).

As shown in Figures 14 and 15, neither the Pleiades nor NGC 2547 shows an obvious mass dependence for the photometric binary frequency. Taken as a group, these plots for Blanco 1, the Pleiades, and NGC 2547 provide strong evidence that at least during an age range of about 30–100 Myr, for stars of about 1 to 3 $M_\odot$ (spectral type A0 to mid-G), there is a strong relationship between debris disk presence and multiplicity in the sense that binary stars (or higher multiples) are less likely to have detected debris disks.

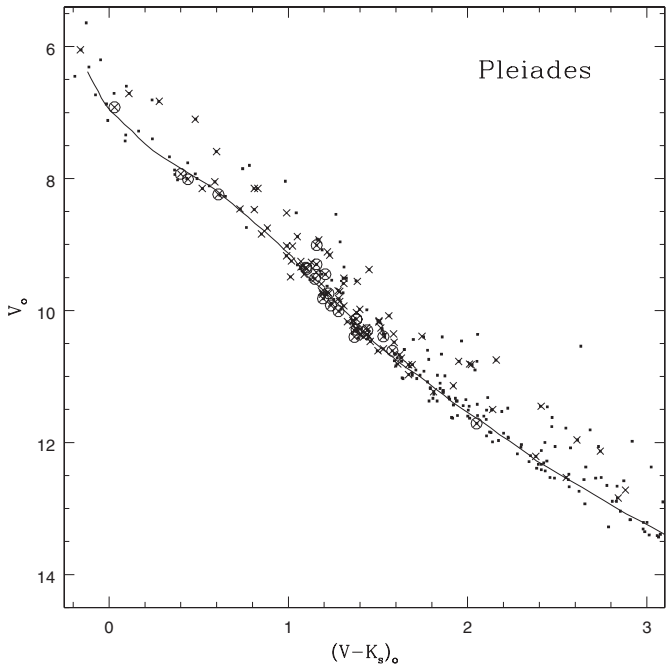

Figure 14. V_o vs. $(V - K_s)_o$ CMD for the Pleiades. Stars with MIPS 24 μm photometry are marked with a cross ("×"); those with 24 μm excesses greater than 15% of the photospheric flux density are circled.

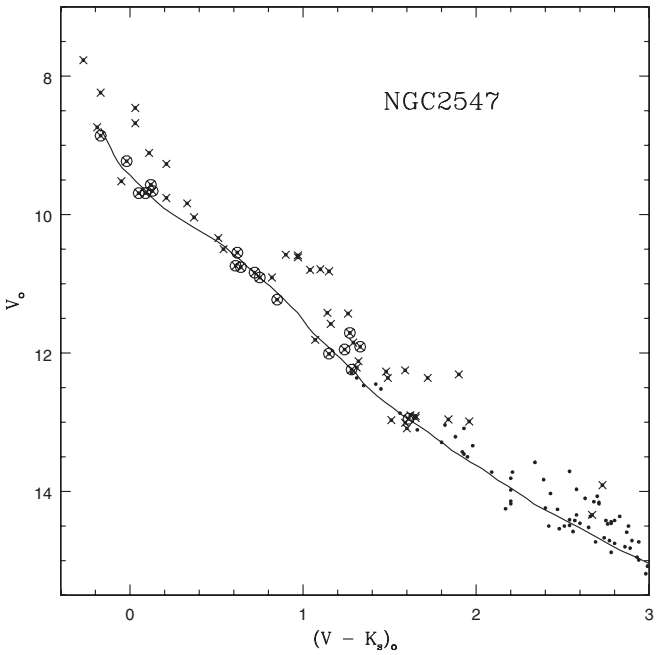

Figure 15. V_o vs. $(V - K_s)_o$ CMD for NGC 2547. Stars with MIPS 24 μm photometry are marked with a cross ("×"); those with 24 μm excesses greater than 15% of the photospheric flux density are circled.

At face value, our result would seem to be in contradiction to the Trilling et al. (2007) determination that binary stars in the field were as likely to have detected debris disks as single stars. However, there are some notable differences in the two studies that may vitiate this seeming contradiction. Most importantly, the stars in the Trilling et al. (2007) sample are comparatively old, with all but three older than 600 Myr and most older than 1 Gyr. For example, if winds are a significant scouring agent, they would be much more effective at the age of our sample than for Trilling's stars. Second (but perhaps connected to the first point), most of the excesses for the Trilling et al. (2007) sample were detected at 70 μm—only 6 of the 69 stars had excesses detected at 24 μm, versus 20 of 50 at 70 μm. Our sample of stars are too distant to detect at 70 μm with our observations. Therefore, we are detecting dust closer to the parent stars than Trilling (on average). Finally, our method of identifying binary stars is much different from that used by Trilling et al. The two studies are therefore probing somewhat different star populations and dust distributions, either of which may affect the conclusions.

7. SUMMARY AND CONCLUSIONS

Our new MIPS data for Blanco 1 adds one more young cluster to the set of open clusters with good data from *Spitzer*. Because of the extensive recent optical photometry and high-resolution spectroscopy obtained by Mermilliod et al. (2008), Cargile et al. (2009), Gonzalez & Levato (2009), and D. J. James et al. (2010, in preparation), we have been able to certify that all of our 25 targeted candidate members are indeed high-probability members of the cluster, and all but one of the serendipitous members for which we were also able to obtain MIPS photometry also have enough published ancillary data to confirm their membership. Eight of the 25 Blanco 1 cluster members for which we have MIPS data of good S/N show significant 24 μm excesses, corresponding to an excess frequency of (32 ± 11)%. This is comparable to the 24 μm excess frequency found in the similar-age Pleiades cluster and is compatible with the trend of debris disk frequency versus age reported in several recent studies. The unusual galactic orbit and paucity of high mass stars in Blanco 1 appear not to have had a strong effect on the processes that influence the formation and evolution of debris disks.

Our most unexpected finding was that we see a much lower IR-excess frequency for photometric binary stars than for stars that lie near the single-star main sequence for members of Blanco 1, NGC 2547, and the Pleiades. This apparent link between binarity and debris disk presence is counter to what was reported for field A and F stars by Trilling et al. (2007), who found no correlation between binarity and IR excess. Because their sample of stars is much older than ours, there may in fact be no contradiction. The disparity of the two results, however, does suggest that further studies with different sample selections would be useful. Assuming that the correlation between binarity and MIPS 24 μm excess is confirmed, the next step would be to determine what types of binaries have the most influence, which will require samples with binary identification and characterization obtained by additional means (radial velocity surveys, AO imaging, etc.).

During the course of our analysis of the Blanco 1 stars, we used MIPS data for stars in the Hyades to provide an accurate template to define the photospheric $V - K_s$ versus $K_s - [24]$ relation for G and K dwarfs. As a result of that analysis, we have identified three Hyades low mass members (vB 19, VA 133, and VA 407) as possible debris disk sources.

This work is based in part on observations made with the *Spitzer Space Telescope*, which is operated by the Jet Propulsion Laboratory, California Institute of Technology under a contract with NASA. Support for this work was provided by NASA through an award issued by JPL/Caltech. Most of the support for this work was provided by the Jet Propulsion Laboratory, California Institute of Technology, under NASA contract 1407. This research has made use of NASA's Star and Exoplanet

Table 3
Pleiades Data

Star Name	$V-K_s$	K_s − [24] exc.	δV	Star Name	$V-K_s$	K_s − [24] exc.	δV	Star Name	$V-K_s$	K_s − [24] exc.	δV
AK1A317	1.18	0.02	0.07	HII0717	0.48	−0.06	0.88	HII1876	0.28	0.01	0.88
AK1A36	1.52	0.05	0.30	HII0727	1.31	0.03	0.41	HII1912	1.17	−0.01	0.41
AK1A56	1.59	0.12	0.36	HII0739	1.45	0.03	1.03	HII1924	1.36	0.07	1.03
AK1A76	1.10	0.28	0.10	HII0885	2.61	0.10	0.67	HII2027	2.01	0.00	0.67
AK1B146	1.31	−0.07	0.49	HII0923	1.38	0.09	0.18	HII2034	2.55	−0.02	0.18
AK1B365	1.28	0.06	0.20	HII0996	1.38	0.22	−0.08	HII2147	2.16	−0.03	−0.08
AK1B560	1.15	0.37	0.06	HII1015	1.42	−0.03	−0.07	HII2172	1.37	0.12	−0.07
AK1B590	1.02	−0.04	0.17	HII1095	2.05	0.28	−0.08	HII2195	0.44	0.27	−0.08
AK1B7	1.29	0.13	0.22	HII1100	2.74	0.13	0.71	HII2278	2.02	0.00	0.71
AK1B8	1.38	0.07	−0.08	HII1101	1.38	0.41	0.08	HII2311	1.81	−0.08	0.08
AKII34	1.22	0.06	0.65	HII1117	1.56	0.08	0.58	HII2341	1.61	0.07	0.58
AKII359	1.46	0.01	−0.04	HII1122	0.99	0.11	−0.06	HII2345	0.99	−0.05	−0.06
AKII383	1.24	0.19	−0.12	HII1132	1.16	3.08	0.30	HII2506	1.36	−0.06	0.30
AKII437	1.19	1.47	−0.13	HII1139	1.02	0.10	−0.08	HII2644	1.67	−0.05	−0.08
AKIII28	1.16	0.00	0.18	HII1182	1.44	−0.01	0.02	HII2786	1.33	−0.04	0.02
HCG131	2.84	−0.05	0.17	HII1200	1.28	0.13	0.09	HII2881	2.41	−0.07	0.09
HCG132	2.88	0.10	0.35	HII1207	1.40	0.02	−0.09	HII3031	0.88	0.03	−0.09
HII0025	1.10	0.15	0.10	HII1266	0.83	−0.01	0.56	HII3097	1.69	0.03	0.56
HII0102	1.75	0.08	0.63	HII1284	0.61	0.32	−0.03	HII3179	1.31	−0.06	−0.03
HII0120	1.63	0.02	0.09	HII1298	2.38	0.05	0.06	Pels7	1.44	0.01	0.06
HII0152	1.50	0.12	−0.08	HII1309	1.07	−0.02	0.02	Pels20	1.37	0.23	0.02
HII0173	1.95	−0.03	0.68	HII1338	0.99	0.03	0.59	Pels23	1.40	0.09	0.59
HII0174	2.14	0.00	0.30	HII1362	0.52	0.06	−0.11	Pels25	1.09	0.03	−0.11
HII0250	1.53	0.10	0.01	HII1380	0.03	0.19	0.11	Pels40	1.29	0.04	0.11
HII0293	1.62	0.02	0.12	HII1384	0.60	−0.01	0.59	Pels58	0.40	1.01	0.59
HII0314	1.59	−0.01	0.24	HII1431	0.11	0.06	0.53	Pels86	1.07	0.11	0.53
HII0344	0.59	0.04	0.11	HII1514	1.45	0.08	0.02	Pels121	1.50	−0.01	0.02
HII0405	1.22	0.01	0.04	HII1613	1.19	0.03	−0.07	Pels124	1.18	0.08	−0.07
HII0489	1.44	0.23	0.08	HII1726	1.23	0.07	0.63	Pels128	1.51	0.16	0.63
HII0514	1.58	0.16	0.09	HII1762	0.81	−0.03	0.52	Pels135	1.13	0.09	0.52
HII0530	0.85	0.09	−0.08	HII1766	1.16	0.52	0.59	Pels146	1.53	0.41	0.59
HII0531	0.73	0.07	0.02	HII1776	1.67	0.11	0.07	Pels150	1.21	0.22	0.07
HII0571	1.92	0.11	0.26	HII1794	1.40	0.03	0.00	Pels173	1.01	0.16	0.00
HII0605	1.05	−0.02	0.41	HII1797	1.28	0.48	−0.10	Pels174	1.38	0.08	−0.10
HII0697	0.81	0.07	0.20	HII1856	1.24	−0.05	−0.08	Tr60	1.08	−0.14	−0.08

Database (NStED) and the Astrophysics Data System (ADS) Abstract Service, and of the SIMBAD database, operated at CDS, Strasbourg, France. This research has made use of data products from the 2MASS, which is a joint project of the University of Massachusetts and the Infrared Processing and Analysis Center, funded by the National Aeronautics and Space Administration and the National Science Foundation. These data were served by the NASA/IPAC Infrared Science Archive, which is operated by the Jet Propulsion Laboratory, California Institute of Technology, under contract with the National Aeronautics and Space Administration. The research described in this paper was partially carried out at the Jet Propulsion Laboratory, California Institute of Technology, under contract with the National Aeronautics and Space Administration.

APPENDIX

PLEIADES AND NGC 2547 COMPARISON SAMPLE

The Pleiades data used for this comparison come from Stauffer et al. (2005), Gorlova et al. (2006), and Sierchio et al. (2010). We included all stars from the Stauffer et al. and Sierchio et al. papers because all of those stars are F, G, and K dwarfs that fall well within our $V-K_s$ color criterion, and all have good S/N photometry. From the Gorlova et al. sample (their Table 2), we exclude the B stars for the reasons stated in Section 6 and we exclude the five stars with $V-K_s > 3.0$ (the uncertainties in their [24] photometry and in the calibration of the photospheric K_s − [24] color make it impossible to know if these stars have excesses or not). For consistency, for all of the stars we use V and K_s photometry from Stauffer et al. (2007) and the 24 μm photometry as reported in the above three papers, and then calculate our own $V-K_s$ color and K_s − [24] excess and the displacement relative to the single star main sequence of Stauffer et al. (2007) using the same procedures as for Blanco 1. Table 3 provides the data for the stars plotted in Figures 12 and 14.

For NGC 2547, we use data from Gorlova et al. (2007). We restrict ourselves to the same $V-K_s$ range as for the Pleiades, for the same reasons. We include candidate cluster members from both Tables 1 and 2 of Gorlova et al. except we eliminate proper motion non-members and stars that have 24 μm data with 1σ uncertainties more than 0.15 mag. We include ID1 and ID8 from the stars with 8 μm excesses in Table 5 of Gorlova et al. but exclude other such stars (IDs 2 and 4 have K-band excesses, and hence we cannot use $V-K_s$ to identify displacement above the main sequence; ID 4 has no K_s − [24] measurement, and ID 7 has $V-K_s = 5.50$). We include all of the probable 24 μm excess stars in Table 5 of Gorlova et al. (2007), except for 08090344−4859210 which has $(V-K_s)_o = 5.37$ and is thus nearly 2.5 mag redder than the reddest Blanco 1 star for which we have MIPS data. We also exclude the stars listed as just having possible 24 μm excesses, because Gorlova et al.

Table 4
NGC 2547 Data

Star Name	$V - K_s$	K_s − [24] exc.	δV	Star Name	$V - K_s$	K_s − [24] exc.	δV
08090250−4858172	1.61	3.64	0.01	08111134−4904442	0.71	0.53	−0.05
08095601−4919299	0.03	−0.10	1.05	08095066−4912493	0.37	0.02	0.15
08100607−4914180	0.05	1.47	−0.13	08094610−4914270	0.54	−0.01	−0.05
08100841−4900434	0.13	1.10	0.10	08102667−4906532	0.51	−0.01	0.06
08084571−4923473	0.62	0.95	0.07	08091401−4904029	0.85	0.14	−0.10
08093671−4911383	0.03	−0.04	0.83	08093053−4920443	0.82	0.07	0.15
08112585−4912288	0.09	0.70	−0.03	08101836−4906461	1.27	0.42	0.50
08092668−4914371	0.59	1.26	−0.15	08102774−4912095	1.15	−0.15	1.10
08100087−4908324	1.04	0.00	0.86	08101165−4922274	1.26	−0.06	0.76
08102082−4903366	0.11	0.02	0.60	08104984−4911258	1.16	0.13	0.37
08103144−4906301	0.21	−0.09	0.66	08085576−4923085	1.33	0.35	0.47
08110323−4900374	0.57	1.09	−0.19	08085649−4923128	1.59	0.29	0.68
08093053−4921563	0.33	0.00	0.28	08100938−4900565	1.90	0.03	1.16
08101673−4915173	0.72	0.79	0.00	08103983−4904377	1.14	−0.02	0.48
08104233−4857253	0.12	0.28	0.17	08101352−4920438	1.10	0.03	1.02
08104662−4917312	0.90	0.09	0.67	08094507−4856307	1.28	0.44	−0.01
08110860−4900161	0.21	−0.05	0.17	08104546−4901068	1.24	0.42	0.19
08085310−4913492	−.05	0.12	−0.21	08103432−4900496	1.07	0.14	−0.07
08093561−4927015	0.97	−0.03	0.83	08101546−4905487	1.72	0.08	0.78

describe these stars as either having distorted shapes at 24 μm or as having 24 flux densities at the level of fluctuations in the nebulosity. For those reasons, Gorlova et al. did not discuss the sources with "possible 24 μm excesses" further in their paper. Because NGC 2547 is significantly younger than the Pleiades, we cannot use the Pleiades single-star main sequence (shifted to NGC 2547 distance) to identify photometric binaries. Instead, we use the entire NGC 2547 candidate members' list to define the single star locus for that cluster and calculate the displacement relative to that locus. Table 4 provides the relevant data for the NGC 2547 stars plotted in Figures 13 and 15.

REFERENCES

Adams, F., Hollenbach, D., Laughlin, G., & Gorti, Uma. 2004, ApJ, 611, 360
Balog, Z., Kiss, L., Vinko, J., Rieke, G., Muzerolle, J., Gaspar, A., Young, E., & Gorlova, N. 2009, ApJ, 698, 1989
Bate, M., Bonnell, I., & Bromm, V. 2003, MNRAS, 339, 577
Beichman, C., et al. 2006, ApJ, 652, 1674
Bertoldi, F. 1989, ApJ, 346, 735
Bessell, M. 2000, PASP, 112, 961
Bryden, G., et al. 2006, ApJ, 636, 1098
Cargile, P., James, D. J., & Platais, I. 2009, AJ, 137, 3230
Carpenter, J., et al. 2008, ApJS, 179, 423
Carpenter, J., et al. 2009, ApJS, 181, 197
Chen, C., Jura, M., Gordon, K., & Blaylock, M. 2005, ApJ, 623, 493
Cieza, L., Cochran, W., & Augereau, J.-C. 2008, ApJ, 679, 720
Currie, T., Plavchan, P., & Kenyon, S. 2008, ApJ, 688, 597
de Epstein, A., & Epstein, I. 1985, AJ, 90, 1211
Dias, W., Alessi, B., Moitinho, A., & Lepine, J. 2002, A&A, 389, 871
Edvardsson, B., Pettersson, B., Hharrazi, M., & Westerlund, B. 1995, A&A, 293, 75
Engelbracht, C., et al. 2007, PASP, 119, 994
Gaspar, A., Rieke, G., Su, K., Balag, Z., Trillling, D., Muzzerole, J., Apai, D., & Kelly, B. 2009, ApJ, 697, 1578
Gautier, N., et al. 2007, ApJ, 667, 527
Gonzalez, J., & Levato, H. 2009, A&A, 507, 541
Gorlova, N., Balog, Z., Rieke, G., Muzerolle, J., Su, K., Ivanov, V., & Young, E. 2007, ApJ, 670, 516
Gorlova, N., Rieke, G., Muzerolle, J., Stauffer, J., Siegler, N., Young, E., & Stansberry, J. 2006, ApJ, 649, 1028
Gorlova, N., et al. 2004, ApJS, 154, 448
Hauschildt, P., Allard, F., & Baron, E. 1999, ApJ, 512, 377
Jeffries, R. D., & James, D. 1999, ApJ, 511, 218
Jeffries, R. D., & Oliveira, J. 2005, MNRAS, 358, 13
Kenyon, S., & Bromley, B. 2004, ApJ, 602, L133
Kenyon, S., & Hartmann, L. 1995, ApJS, 101, 117
Lada, E., Depoy, D., Evans, N., & Gatley, I. 1991, ApJ, 371, 171
Makovoz, D., & Marleau, F. 2005, PASP, 117, 1113
Mermilliod, J.-C., Platais, I., James, D. J., Grenon, M., & Cargile, P. 2008, A&A, 485, 95
Meyer, M., et al. 2006, PASP, 118, 1690
Micela, G., Sciortino, S., Favata, F., Pallavicini, R., & Pye, J. 1999, A&A, 344, 83
Moraux, E., Bouvier, J., Stauffer, J., Barrado y Navascues, D., & Cuillandre, J.-C. 2007, A&A, 471, 499
Motoyama, K., Umemoto, T., & Shang, H. 2007, A&A, 467, 657
Oort, J., & Spitzer, L. 1955, ApJ, 121, 60
Panagi, P., & O'Dell, M. 1997, A&AS, 121, 213
Panagi, P., O'Dell, M., Collier Cameron, A., & Robinson, R. 1994, A&A, 292, 439
Papovich, C., et al. 2004, ApJS, 154, 70
Perry, C. L., Walter, D. K., & Crawford, D. L. 1978, PASP, 90, 81
Perryman, M., et al. 1997, A&A, 323, L49
Pillitteri, I., Micela, G., Sciortino, S., Damiani, F., & Harnden, R. 2004, A&A, 421, 175
Pillitteri, I., Micela, G., Sciortino, S., & Favata, F. 2003, A&A, 399, 919
Plavchan, P., Jura, M., & Lipscy, S. 2005, ApJ, 631, 1161
Plavchan, P., Werner, M., Chen, C., Stapelfeldt, K., Su, K., Stauffer, J., & Song, I. 2009, ApJ, 698, 1068
Porras, A., Christopher, M., Allen, L., Di Francesco, J., Megeath, S., & Myers, P. 2003, AJ, 126, 1916
Rebull, R., et al. 2008, ApJ, 681, 1484
Rieke, G., et al. 2004, ApJS, 154, 25
Rieke, G., et al. 2005, ApJ, 620, 1010
Schmidt-Kaler, T. H. 1982, in Physical Parameters of the Stars, in Landolt Börnstein, ed. K.-H. Hellwege (New Series, Vol. VI, 2b; Berlin: Springer), 1
Siegler, N., Muzerolle, J., Young, E., Rieke, G., Mamajek, E., Trilling, D., Gorlova, N., & Su, K. 2007, ApJ, 654, 580
Sierchio, J., Rieke, G., Su, K., Plavchan, P., Stauffer, J., & Gorlova, N. 2010, ApJ, 712, 1421
Skrutskie, M., et al. 2006, AJ, 131, 1163
Stauffer, J. R., et al. 2005, AJ, 130, 1834
Stauffer, J. R., et al. 2007, ApJS, 172, 663
Su, K., et al. 2006, ApJ, 653, 675
Trilling, D., et al. 2007, ApJ, 658, 1289
Werner, M., et al. 2004, ApJS, 154, 1
Westerlund, B., Garnier, R., Lundgren, K., Pettersson, B., & Breysacher, J. 1988, A&AS, 76, 101